Modulated phases in multicomponent fluid membranes

P. B. Sunil Kumar, G. Gompper, and R. Lipowsky
Max-Planck-Institut für Kolloid-und Grenzflächenforschung, Am Mühlenberg, Haus 2, 14476 Golm, Germany
(Received 23 November 1998; revised manuscript received 20 May 1999)

We investigate the behavior of flexible two-component bilayer and three-component monolayer membranes. The components are assumed to have different spontaneous curvatures, and to mutually phase separate in planar membranes. As a function of temperature, lateral tension and bending rigidity, a rich phase behavior is obtained. In particular, we find three different types of modulated phases. In symmetric bilayers, the excess component assembles at the boundary between oppositely curved domains; in sufficiently asymmetric bilayers, the excess component is found to preferentially assemble in a single layer, with no tendency for segregation to the domain boundaries. We show that the phase behavior of three-component monolayer strongly resembles the behavior of two-component bilayers. In fact, in a certain, restricted region of parameter space, the two models can be shown to be equivalent. [S1063-651X(99)07210-4]

PACS number(s): 87.16.Dg, 64.60.−i, 68.10.−m, 82.65.Dp

I. INTRODUCTION

Due to strong hydrophobic interactions, amphiphiles such as phospholipids and surfactants spontaneously aggregate in water to form bilayer membranes. These membranes typically have fluidlike in-plane order and are very flexible, with their shapes and fluctuations controlled by the bending energy. In the case of lipid membranes, the bending rigidity $\kappa \approx 10^{-12}$ erg is large enough to stabilize structures which are much larger ($\sim 10-20$ μm) than the molecular scale ($\sim 10-20$ Å). The conformations of such membranes have been studied both experimentally and theoretically in considerable detail recently [1–3].

Most of the experimental studies on lipid membranes have concentrated on systems made of only one type of lipid. On length scales larger than the bilayer thickness, the equilibrium conformations of laterally homogeneous membranes are determined by their bending elasticity, so that the membranes can be described as a two-dimensional elastic sheet. Extensive studies [4–7] of such theoretical models have resulted in complicated shape phase diagrams.

Biological membranes, however, are complex mixtures of lipid species, which vary with respect to both the lipid head groups and the associated alkyl chains [8]. It is therefore important to examine the properties of fluid membranes made of a simple mixture of pure lipids to get an idea about the more complex phenomena encountered in biomembranes. The presence of more than one component in a fluid membrane leads to the possibility of phase separation and domain formation within the membrane [9,3]. The additional degrees of freedom introduced by the phase segregation can significantly alter the shape phase diagram of membranes, since the line tension between the phases and the dependence of curvature on the local composition become important in determining the equilibrium conformations [3].

Theoretical studies [10–19] of multicomponent membranes have so far been limited to the case of two-component systems. For *two-component monolayers*, which are composed of molecules with different head group areas and tail sizes, the most common approach is to couple the spontaneous curvature to the local composition linearly, i.e., to express the spontaneous curvature as a linear superposition of the spontaneous curvatures of the two components. In the case of binary mixtures of lipids, phase diagrams have been calculated for two limiting cases. In the *strong segregation limit* [11,12,16,13], the correlation length for concentration fluctuations is comparable to the molecular scale, so that the domain boundary is sharp and each domain consists mainly of a single species of molecules. This limit applies at low temperatures and large line tensions. In the *weak segregation limit* [10,15], on the other hand, there is only a small excess of one component in each domain; the domain boundaries are broad in this case, and the line tension is small. The weak segregation limit usually applies to systems in the vicinity of a critical point.

For *two-component bilayers*, the dependence of the spontaneous curvature on composition is derived from the properties of the two monolayers [20]. The linear approximation of the composition dependence of monolayers mentioned above leads immediately to a coupling of the membrane curvature to the *difference* in compositions between the two halves of the bilayer [18]. It is important to realize that domains in bilayers can either extend across both monolayers, or can be confined to a single monolayer [11]. We will show in this paper that the interaction of the domains of the two monolayers gives rise to alternative types of modulated phases. We want to mention parenthetically that the bilayer structure of the membrane also leads to other possible shape transitions. For example, in phase-separating fluid bilayers the two phases can coexist on opposite sides of a bilayer resulting in a stable one-phase vesicle region [20,17].

In the case of *three-component monolayers*, the situation is more complicated. In general, the local mean curvature is coupled to *two* composition variables. Only for special choices of spontaneous curvatures of the three components does the composition dependence of the curvature coupling again become relatively simple. This is the case, for example, when the spontaneous curvatures of two components are equal in magnitude and opposite in sign, while the third component has vanishing spontaneous curvature.

In this paper we will consider two-component bilayers (Sec. II) and three-component monolayers (Sec. III). We

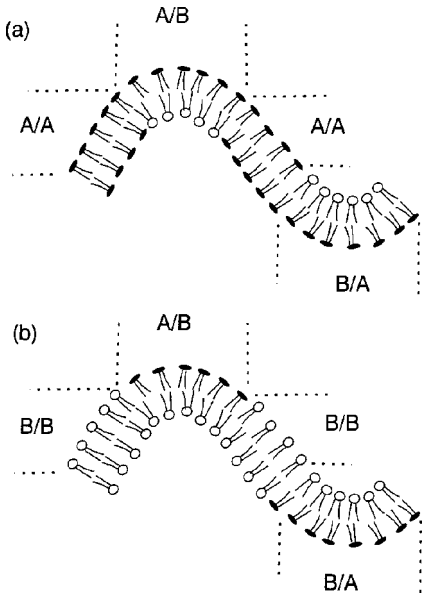

FIG. 1. Schematic representation of a two component bilayer membrane with curvature coupled to the local concentration. (a) Excess of the *A* component. (b) Excess of the *B* component.

show that both kinds of membranes have a very rich phase behavior. In fact, we observe that the phase diagrams of the two models show remarkable similarities. This can be seen by considering the case of a bilayer made of two amphiphiles *A* and *B*, as shown schematically in Fig. 1. In the case where *A* is the majority component [Fig. 1(a)], there are three different local combinations of *up/down* composition—*A*/*B*, *B*/*A*, and *A*/*A*—with different curvature energies. If we identify the *A*/*B*, *B*/*A*, and *A*/*A* regions with three different types of molecules, we can replace the bilayer by a three-component monolayer. We show in Sec. IV that the phase diagrams of the two models are indeed very similar. In fact, in a restricted region of parameter space, a direct mapping between these two models exists.

II. TWO-COMPONENT BILAYERS

Let us first consider bilayers made of two types of lipids. We start with a lattice model for a *flat* two-component bilayer made of two interacting monolayers. The Hamiltonian is taken to be

$$\mathcal{H}=J_1\sum_{\langle ij\rangle}(\sigma_i'\sigma_j'+\sigma_i''\sigma_j'')+J_2\sum_i \sigma_i'\sigma_i''+J_3\sum_{\langle ij\rangle}(\sigma_i'\sigma_j''+\sigma_i''\sigma_j')-\sum_i[\tilde{\eta}(\sigma_i'-\sigma_i'')+\tilde{\Delta}(\sigma_i'+\sigma_i'')], \tag{1}$$

where $\sigma_i=+1(-1)$ for $A(B)$ molecules occupying site i of a triangular lattice. The spin variables of the upper and lower monolayers are denoted by σ_i' and σ_i'', respectively. We distinguish between the three different interactions of the lipids, the in-plane interaction J_1, the direct interplane interaction J_2 and the diagonal interplane interaction J_3.

We want to remark parenthetically that it is useful to start with a lattice model (rather than a continuum model), because this will allow us to derive a close correspondence between two-component bilayers and three-component monolayers in Sec. IV below.

We now introduce two continuum variables $\phi(\mathbf{r}_i)=(\langle\sigma_i'\rangle-\langle\sigma_i''\rangle)/2$ and $\psi(\mathbf{r}_i)=(\langle\sigma_i'\rangle+\langle\sigma_i''\rangle)/2$ to define the local composition of the bilayer. Equation (1) can then be written in the continuum limit as

$$\mathcal{H}=\int d^2r((6J_1+J_2+6J_3)\phi^2+(6J_1-J_2-6J_3)\psi^2+\tfrac{3}{4}(J_1-J_3)(\nabla\phi)^2+\tfrac{3}{4}(J_1+J_3)(\nabla\psi)^2-\eta\phi-\Delta\psi). \tag{2}$$

The total mean-field free-energy functional for the in-plane ordering is then

$$F_{plane}(\phi,\psi)=\int d^2r\left[\frac{b_1'}{2}(\nabla\phi)^2+\frac{b_2'}{2}(\nabla\psi)^2+f_{plane}(\phi,\psi)-\eta\phi-\Delta\psi\right] \tag{3}$$

with

$$f_{plane}(\phi,\psi)=\frac{a'}{2}\phi^2+\frac{b'}{2}\psi^2+\frac{T}{2}[(1+\psi+\phi)\ln(1+\psi+\phi)+(1-\psi-\phi)\ln(1-\psi-\phi)+(1+\psi-\phi)\times\ln(1+\psi-\phi)+(1-\psi+\phi)\ln(1-\psi+\phi)] \tag{4}$$

where $a'=2(6J_1+J_2+6J_3)$, $b'=2(6J_1-J_2-6J_3)$, $b_1'=\frac{3}{2}(J_1-J_3)$, and $b_2'=\frac{3}{2}(J_1+J_3)$.

For small deformations from the planar state, we can use the Monge representation to describe the membrane shape. The curvature energy is then given by

$$F_{curv}(h)=\int d^2r\left[\frac{\kappa}{2}(\nabla^2h)^2+\frac{\sigma}{2}(\nabla h)^2\right]. \tag{5}$$

We consider the case where the *A*-rich and *B*-rich regions favor opposite curvatures. Such a bias in curvature is natural when the volumes occupied by the polar head and hydrophobic tail of the two types of lipid molecules are different. This is shown schematically in Fig. 1. The demixing of lipids can then lead to three distinct regions. When both leaves have the same composition, the bilayer membrane preferentially remains flat and has no net spontaneous curvature. Regions with a difference in composition of the two layers, on the other hand, will have positive or negative curvatures [11,17]. If the composition dependence of the spontaneous curvature of a monolayer is assumed to be linear [10], i.e., the spontaneous curvature is expressed as a linear superposition of the spontaneous curvatures of the two components, the interaction energy has the form [18]

$$F_{c-\phi}(\phi,h)=C\int d^2r(\nabla^2h)\phi. \tag{6}$$

By combining Eqs. (2), (4), (5), and (6), we get the effective free-energy functional

$$F(\phi,\psi,h)=\int d^2r\left[\frac{\kappa}{2}(\nabla^2 h)^2+\frac{\sigma}{2}(\nabla h)^2 + C\phi\nabla^2 h+\frac{b_1'}{2}(\nabla\phi)^2+\frac{b_2'}{2}(\nabla\psi)^2 + f_{plane}(\phi,\psi)-\eta\phi-\Delta\psi\right]. \quad (7)$$

In the mean-field approximation, the equation for the membrane shape is obtained by setting $\delta F/\delta h_q=0$, where h_q is the Fourier transform of $h(x,y)$; this gives

$$h_q=\frac{C\phi_q}{(\sigma+\kappa q^2)}. \quad (8)$$

In order to keep the analysis as simple as possible, we now neglect the $(\nabla\psi)^2$ term in Eq. (3). This choice is motivated by the fact that the variation of the total concentration $\psi(\mathbf{r})$ should usually be smaller than the variation of the concentration difference $\phi(\mathbf{r})$. Furthermore, when the interplane interaction J_3 is chosen to be of opposite sign of J_1—to favor interplane attraction of unlike lipids in the two layers—the parameter $b_2'=(J_1+J_3)$ is smaller than $b_1'=(J_1-J_3)$, so that the $(\nabla\phi)^2$ term should be the dominant gradient contribution. By inserting Eq. (8) into Eq. (7) and expanding the resulting expression in powers of q up to order q^4, we then find the effective free-energy functional

$$F_{eff}(\phi,\psi)=\int d^2q\left[\left(\frac{\kappa C^2}{2\sigma^2}q^4-\frac{(C^2-b_1'\sigma)}{2\sigma}q^2\right)\phi_q^2\right] + \int d^2r[f_{plane}(\phi,\psi)-\eta\phi-\Delta\psi]. \quad (9)$$

We want to remark parenthetically that the case of $J_3=0$ and $J_2\neq 0$, in which $b_1'=b_2'$ and $a'\neq b'$, has been studied in Ref. [19] for equal chemical potential of the two components, i.e., in the $\eta=0$ subspace of the phase diagram. The phase behavior of the two models in this subspace is found to be qualitatively the same.

We now employ a single-mode approximation, in which the Fourier representations of ϕ and ψ are truncated after the terms with the smallest nonzero wave vector. The magnitude q^* of this wave vector is obtained by minimizing F_{eff} with respect to q. Due to the omission of the $(\nabla\psi)^2$ term in Eq. (3), the equation for q^* can be solved explicitly, and leads to

$$q^{*2}=\frac{(C^2-b_1'\sigma)\sigma}{2C^2\kappa}. \quad (10)$$

This is the same expression as obtained in Ref. [10] for the case of two-component monolayers. In the limit of small lateral tension σ, the Monge parametrization is no longer appropriate since domains have the tendency to form small buds [11]. This is reflected in the behavior of q^* which vanishes identically in the limit of zero lateral tension, $\sigma=0$; all modulated phases are therefore the result of the competition between spontaneous curvature and lateral tension. The lateral tension σ and the line tension—characterized by b_1'—have opposite effects on q^*. The wave number q^* decreases with increasing b_1', since a higher line tension implies a larger distance between domain boundaries. An increase of σ (for $\sigma<C^2/2b_1'$), on the other hand, leads to a flattening of the membrane and therefore to a smaller domain size.

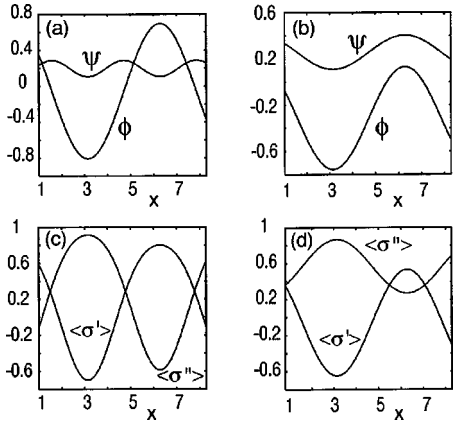

FIG. 2. Modulations of the ϕ and ψ fields as a function of distance x in the (a) L_{II} and (b) L_I stripe phases. Note that in the L_{II} phase the total A-concentration, ψ, peaks at the *domain boundary* between A/B and B/A regions, while in the L_I phase the maximum of the total A-concentration occurs inside the A/B domains. Modulations of the A-concentration of the up ($\langle\sigma'\rangle$) and down ($\langle\sigma''\rangle$) layers in the (c) L_{II} and (d) L_I stripe phases.

We want to emphasize that the use of the single-mode approximation restricts our calculations to the weak segregation limit. Therefore, the temperature in the free energy functional (4) has to be so large that the extrema of the concentration profiles, compare Fig. 2, do not approach their boundary values too closely. Our results could be extended to lower temperatures and larger line tensions by employing more modes in the Fourier expansion of the concentration profiles. This has been done, for example, in the case of diblock-copolymer melts [21].

Finally, we substitute $q=q^*$ in F_{eff} to obtain the effective free-energy density

$$f_{eff}=-\frac{z}{2}a_1\phi_{q^*}^2+\frac{1}{A_0}\int d^2r f_{plane}(\phi,\psi), \quad (11)$$

where z is the number of different wave vectors of length q^* ($z=1$ for a lamellar, $z=2$ for a square and $z=3$ for a hexagonal phase), A_0 is the membrane area, and

$$a_1=\frac{(C^2-b_1'\sigma)^2}{8\kappa C^2}. \quad (12)$$

This is the starting point for our investigation of the stability of different modulated phases. It should be mentioned that in an experimental situation a change in a_1 is most easily achieved by changing the surface tension σ.

To calculate the phase diagram, we compare the free energy of the following phases:

(1) Stripe phase L_I:

$$\phi = \phi_0 + \phi_{q*}\cos(q^*x),$$

$$\psi = \psi_0 + \psi_{q*}\cos(q^*x). \tag{13}$$

(2) Stripe phase L_{II}:

$$\phi = \phi_0 + \phi_{q*}\cos(q^*x),$$

$$\psi = \psi_0 + \psi_{q*}\cos(2q^*x). \tag{14}$$

Note that unlike in the case of two-component monolayers, we have the possibility of two different stripe phases here. The modulations of the ϕ and ψ fields in the coexisting region of the two stripe phases L_I and L_{II} are shown in Fig. 2. In the L_{II} phase, see Figs. 2(a) and 2(c), regions of larger ψ values are located at the *domain boundary* between stripes with positive and negative ϕ values. Since $\langle\sigma'\rangle = (\psi+\phi)$ and $\langle\sigma''\rangle = (\psi-\phi)$, this corresponds to a structure with (approximately flat) regions, in which the *same* component is enriched on both sides of the bilayer, occurring at the domain boundary between (oppositely curved) regions, in which the A concentration is increased in the top and bottom layers, respectively—compare Figs. 1 and 2(c). This phase is different from the L_I structure shown in Figs. 2(b) and 2(d), where the total A-concentration peaks *inside* the A/B domains.

Similarly, there is the the possibility of two different square phases, and three different hexagonal phases.

(3) Square phase S_I:

$$\phi = \phi_0 + \phi_{q*}[\cos(q^*x) + \cos(q^*y)],$$

$$\psi = \psi_0 + \psi_{q*}[\cos(q^*x) + \cos(q^*y)]. \tag{15}$$

(4) Square phase S_{II}:

$$\phi = \phi_0 + \phi_{q*}[\cos(q^*x) + \cos(q^*y)],$$

$$\psi = \psi_0 + \psi_{q*}[\cos(2q^*x) + \cos(2q^*y)]. \tag{16}$$

(5) Hexagonal phase H_I:

$$\phi = \phi_0 + \phi_{q*}\sum_{i=1}^{3}\cos(\mathbf{k}_i\cdot\mathbf{r}),$$

$$\psi = \psi_0 + \psi_{q*}\sum_{i=1}^{3}\cos(\mathbf{k}_i\cdot\mathbf{r}), \tag{17}$$

where $\mathbf{k}_1 = q^*\hat{\mathbf{x}}$, $\mathbf{k}_2 = (q^*/2)(-\hat{\mathbf{x}} + \sqrt{3}\hat{\mathbf{y}})$ and $\mathbf{k}_3 = (q^*/2)(-\hat{\mathbf{x}} - \sqrt{3}\hat{\mathbf{y}})$ with unit vectors $\hat{\mathbf{x}}$ and $\hat{\mathbf{y}}$;

(6) Hexagonal phase H_{II}:

$$\phi = \phi_0 + \phi_{q*}\sum_{i=1}^{3}\cos(\mathbf{k}_i\cdot\mathbf{r}),$$

$$\psi = \psi_0 + \psi_{q*}\sum_{i=1}^{3}\cos(2\mathbf{k}_i\cdot\mathbf{r}). \tag{18}$$

(7) Hexagonal phase H_{III}:

$$\phi = \phi_0 + \phi_{q*}\sum_{i=1}^{3}\cos(\mathbf{k}_i\cdot\mathbf{r}),$$

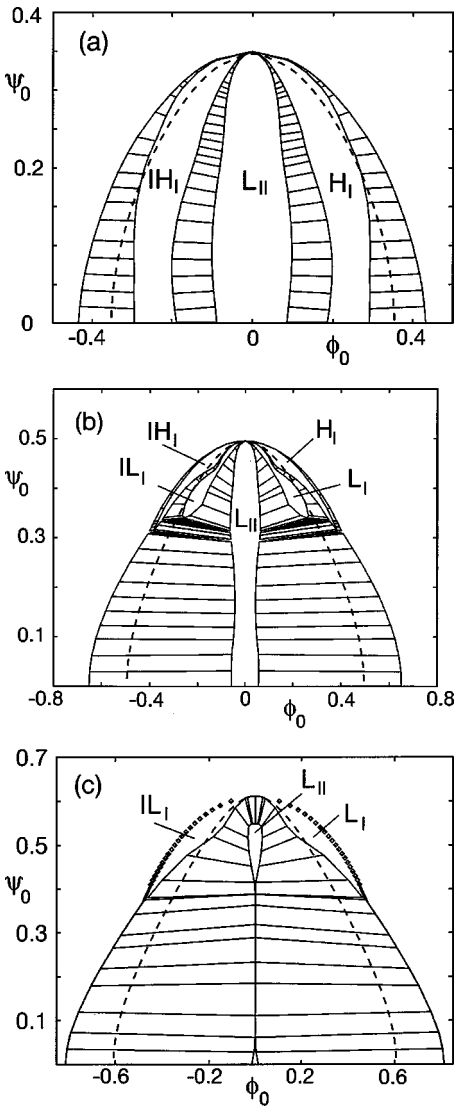

FIG. 3. Phase diagram of the two component bilayer for $a' = -2.7$, $b' = 0$, $a_1' = 0.24$ and three different temperatures (a) $T = 1.4$, (b) $T = 1.2$, and (c) $T = 1.0$. In (c), the one-phase region of L_{II} becomes very narrow for $\psi \lesssim 0.4$, but persists all the way to $\psi = 0$. The lines marked by diamonds ($\diamond$) indicate second-order transitions. The dashed lines are the spinodals of the metastable S_{II} square and L_{II} lamellar phases.

$$\psi = \psi_0 + \psi_{q*}\sum_{i=1}^{3}\cos(\sqrt{3}\mathbf{p}_i\cdot\mathbf{r}). \tag{19}$$

where, $\mathbf{p}_1 = (q^*/2)(\sqrt{3}\hat{\mathbf{x}} + \hat{\mathbf{y}})$, $\mathbf{p}_2 = (q^*/2)(-\sqrt{3}\hat{\mathbf{x}} + \hat{\mathbf{y}})$ and $\mathbf{p}_3 = q^*\hat{\mathbf{y}}$.

(8) Disordered phases (D) with $\phi_q = 0$, $\psi_q = 0$.

Finally, we distinguish between hexagonal phases (H)—with A/B domains (A excess in the top layer, B excess in the bottom layer) in a B/A majority phase—and inverse hexagonal (IH) phases — with B/A-domains in an A/B majority phase. A similar distinction is made for the L_I and S_I phases.

The resulting phase diagram is shown in Fig. 3 in the (ϕ,ψ) plane for three different values of temperature. At high temperature [Fig. 3(a)], we find three modulated phases,

the hexagonal phase H_I, the inverted phase IH_I, and the symmetric stripe phase L_{II}, as well as the homogeneous disordered phase. For $\psi_0 \lesssim 0.35$, this is the same behavior as for two-component monolayers [10]. The modulated phases cease to exist for $\psi_0 \gtrsim 0.35$. For lower temperature [Fig. 3(b)], the new, asymmetric stripe phases L_I and IL_I appear between the hexagonal and the disordered phase. The hexagonal phase disappears as the temperature is lowered further [Fig. 3(c)]. Simultaneously, the line of transitions between the L_I and the disordered phases changes from first order at small ψ to second order at larger ψ values. For $\phi \simeq 0$, we believe that the L_{II} phase coexists with the D phase. However, numerically we cannot exclude the possibility that the critical line of the L_I-to-L_{II} transitions just touches the $L_{II} - D$ binodal.

In the weak-segregation limit studied here, the square phases S_I and S_{II} were found not to be stable anywhere in the phase diagram. However, the square phase S_{II} exists as a metastable phase in the center of the phase diagram, as indicated by the dashed lines in Fig. 3. The spinodals of this metastable phase are identical with the spinodals of the metastable L_{II} phase. In the strong-segregation limit, the stability of the S_{II} phase remains to be investigated.

III. THREE-COMPONENT MONOLAYERS

Our motivation for studying the phase behavior of three-component monolayers is twofold. First, a three-component system is one step further towards the complexity of biological systems. Second, there is an interesting correspondence between two-component bilayers and three-component monolayers, as mentioned briefly in the introduction. The schematic representation of Fig. 1 shows a surface with *three* different favored curvatures — depending on three different combinations of A and B molecules in the two sheets of the bilayer membrane. If we assume the two flat regions of the bilayer (A/A and B/B in Fig. 1) to have the same energy, the bilayer model can be replaced by a monolayer model with three components.

Before we discuss the mapping of the two models in more detail, we want to investigate the three-component monolayer in its own right, in particular the possible modulated phases that can result from the demixing of the constituent components in a three-component membrane. We restrict our study to the case of almost planar membranes as before.

The generic lattice model to study the behavior of ternary systems is the Blume-Emery-Griffiths model [22]. In the spin representation, the most general Hamiltonian for a system with nearest-neighbor pair interactions only is given by

$$\mathcal{H}(S) = -\sum_{\langle ij \rangle} \left[JS_iS_j + KS_i^2S_j^2 + L(S_i^2S_j + S_iS_j^2) \right] + \sum_i \left[DS_i^2 + HS_i \right], \tag{20}$$

where the spin variable $S_i = 1, -1, 0$ correspond to site i of a triangular lattice being occupied by the A, B, or C molecules, respectively. In the mean-field approximation, the free-energy density of homogeneous phases in this model is given by [23]

$$f(x_1,x_2,x_3) = ax_1x_2 + bx_1x_3 + cx_2x_3 + T[x_1 \ln(x_1) + x_2 \ln(x_2) + x_3 \ln(x_3)], \tag{21}$$

where x_1, x_2, and x_3 are the mole fractions of components A, B, and C, respectively, which satisfy $x_1 + x_2 + x_3 = 1$. The relation of the parameters used in Eqs. (20) and (21) is given by [23]

$$a = 12J, \quad b = 3(J + K + 2L), \quad c = 3(J + K - 2L). \tag{22}$$

We now introduce the relative composition of the A and B molecules, $\phi = x_1 - x_2 = \langle S \rangle$, and $\rho = x_3 = 1 - \langle S^2 \rangle$ as the two order parameters such that $-1 < \phi < 1$ and $0 < \rho < 1$. In this paper we consider only the symmetric case, where the free energy is symmetric in ϕ (A-B symmetry). In this case, one has $L = 0$ and $b = c$, and the free-energy density can be written as

$$f(\phi,\rho) = \frac{a}{4}(1 - \rho + \phi)(1 - \rho - \phi) + b\rho(1 - \rho) + T\frac{(1 - \rho + \phi)}{2} \ln(1 - \rho + \phi) + T\frac{(1 - \rho - \phi)}{2} \ln(1 - \rho - \phi) + T\rho \ln \rho. \tag{23}$$

The free-energy functional of an *inhomogeneous*, planar monolayer then reads

$$F_i = \int d^2r \left[\frac{b_1}{2}(\nabla\phi)^2 + \frac{b_2}{2}(\nabla\rho)^2 + f(\phi,\rho) - \mu\phi - \lambda\rho \right] \tag{24}$$

to lowest order in a gradient expansion, where [23]

$$\lambda = D - 3(J + K). \tag{25}$$

We assume the shape of the membrane to depend on the local composition in such a way that an excess of component A favors positive mean curvature of the membrane, an excess of B favors negative mean curvature (of equal magnitude), and an excess of component C favors zero mean curvature. In this case, the coupling between the composition and the mean curvature has the same form as in the case of bilayers, compare Eq. (6), and is given by

$$F_{c-\phi} = C \int d^2r (\nabla^2 h)\phi. \tag{26}$$

In the analysis described below, we set again $b_2 = 0$, for simplicity. Since there is no coupling between the ρ field and the mean curvature in Eq. (26), the equations for $h_q(\phi)$ and the most unstable wave vector are the same as in the bilayer case, see Eqs. (8) and (10) of the previous section.

We consider the same types of phases as in the case of bilayers. There are two possible stripe phases, L_I and L_{II}. The stripe phase L_{II} has C-rich regions sandwiched between stripes of A-rich and B-rich regions, while the L_I phase has alternating stripes of A-rich and $B + C$-rich regions. Similarly, the hexagonal phases H_I, H_{II}, and H_{III} and the square

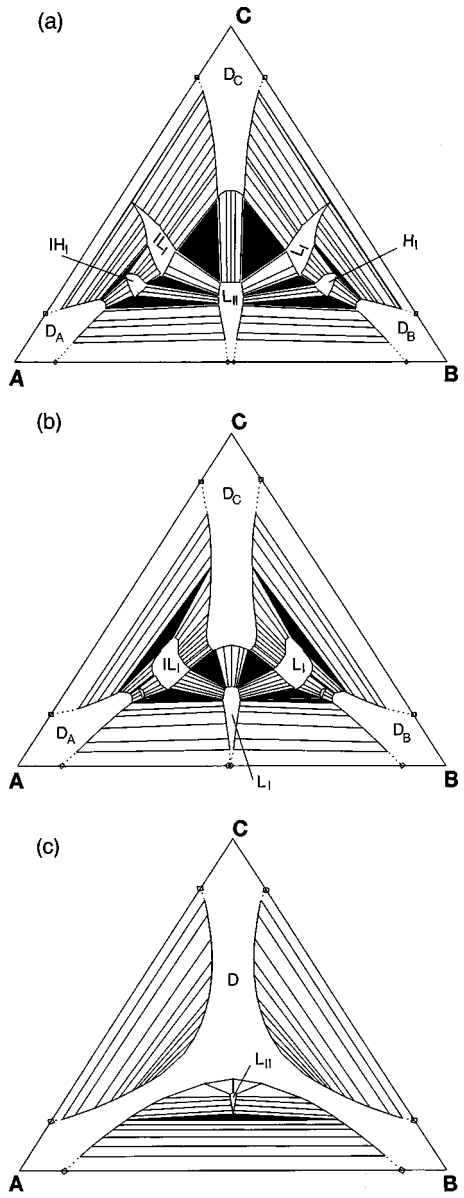

FIG. 4. Phase diagram of the three-component monolayer for $a=2.7$, $b=2.5$, $T=1.0$. (a) $a_1=0.12$, (b) $a_1=0.06$, and (c) $a_1=0.01$. Black areas indicate three-phase regions.

phases S_I and S_{II} have large C concentrations either inside the B-rich domains, or at the boundary between A- and B-rich domains. Also, there are three homogeneous A-rich, B-rich, and C-rich disordered phases. Finally, we distinguish again between hexagonal phases (H)—with A-domains in a B-rich majority phase—and inverse hexagonal (IH) phases—with B-domains in a A-rich majority phase. A similar distinction is also made for the L_I and S_I phases.

The resulting phase diagram is shown in Fig. 4 for three different values of the parameter a_1. For large values of a_1, see Fig. 4(a), there are three distinct modulated phases. All the phases are separated by first-order transitions. Since the A-rich and B-rich regions like to curve in opposite directions, the most probable phases for $\phi_0 \approx 0$ are the symmetric L_{II} and S_{II} phases. We see from Fig. 4 that at low values of ρ_0 and ϕ_0 indeed the L_{II} phase appears. With increasing concentration of A or B components, the L_{II} phase goes over into

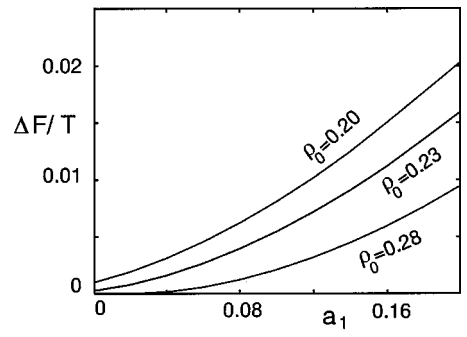

FIG. 5. Difference in reduced free energy, $\Delta F/T$, for the three-component monolayer between the square phase S_{II} and the stripe phase L_{II} as a function of a_1 for the parameters $a=5.2$, $b=1.35$, $T=1.0$.

the B-rich disordered phase (D_B) for $\phi_0 \searrow -1$ and to the A-rich disordered phase (D_A) for $\phi_0 \nearrow 1$. The L_{II} phase exists all the way down to the two-component limit with $\rho_0=0$. Since equal concentration of up and down regions cannot be arranged on a triangular lattice, hexagonal phases are more likely to be stable for asymmetric composition of A and B. In the H_I (IH_I) phase, the C component is mixed with $A(B)$. An increase in ρ_0 makes the background flatter and increases the stability of the hexagonal phases; this leads to a change of the L_{II}-D_A transition into a L_{II}-H_I transition. The second lamellar phase L_I (IL_I)—with alternating stripes of $A(B)$ and C mixed with $B(A)$—appears for $\rho_0 \geqslant 0.5$.

At the boundaries of the three-phase triangle, the concentration of one of the components is zero. This enables us to use two-component models to study the phase behavior along these lines. The points marked on the boundary are obtained from such calculations. We see that the phase boundaries inside the Gibbs triangle connects smoothly (the dotted lines in Fig. 4) to the two-component limits.

With decreasing a_1 the region of stability for the modulated phases shrinks. From Fig. 4 we see that first the hexagonal phase and then the stripe phase L_I disappears. For a_1 close to zero [Fig. 4(c)] the Gibbs triangle shows—except for a small region of L_{II}—only coexistence of disordered phases ending in critical points.

The above calculation can also be done using a Landau expansion of $f(\phi,\rho)$ of the form

$$f_l(\phi,\rho)=\left(-\frac{a}{4}+2T\right)\phi^2+\left(\frac{a}{4}-b+T\right)\rho^2 + T\left(\tfrac{2}{3}\phi^4+\tfrac{4}{3}\rho^4+2\rho\phi^2+4\phi^2\rho^2\right). \quad (27)$$

The resulting phase diagram is similar to Fig. 4 in the central region, but differs appreciably towards the two-component limits.

For the whole parameter space investigated the square phase was conspicuously absent, just as in the case of two-component bilayers. From symmetry considerations, this phase should be most stable along the $\phi_0=0$ line. In Fig. 5 we show a comparison of the free-energy difference ΔF of the S_{II} and L_{II} phases for different values of ρ_0 and a_1. For a given value of ρ, this free-energy difference increases in favor of the L_{II} phase with increasing a_1. Although this difference in free energy tends to zero with decreasing ρ and

a_1, the local minimum of the free-energy functional, which corresponds to the square phase, disappears before ΔF reaches zero. The square phase is therefore only metastable in this model.

IV. MAPPING OF THREE-COMPONENT MONOLAYERS TO TWO-COMPONENT BILAYERS

Let us now look at the correspondence between the three-component monolayer and the two-component bilayer in more detail. With the identification

$$S_j=(\sigma_j'-\sigma_j'')/2 \tag{28}$$

between the variables σ_j' and σ_j'' for the two-component bilayer and the variable S_j for the three-component monolayer models, we can write the partition function of the planar three-component model as

$$\sum_{\{S_i\}}\exp[-\beta\mathcal{H}\{S_i\}]=\sum_{\{S_i\}}\sum_{\{\sigma_i',\sigma_i''\}}\prod_i[(2-S_i^2)^{-1}\delta(S_i-(\sigma_i'-\sigma_i'')/2)]\exp[-\beta\mathcal{H}\{\sigma_i',\sigma_i''\}]$$

$$=\sum_{\{\sigma_i',\sigma_i''\}}\prod_i 2^{(\sigma_i'-\sigma_i'')^2/4-1}\exp[-\beta\mathcal{H}\{\sigma_i',\sigma_i''\}]=\sum_{\{\sigma_i',\sigma_i''\}}\exp[-\beta\tilde{\mathcal{H}}\{\sigma_i',\sigma_i''\}] \tag{29}$$

with an effective Hamiltonian

$$\tilde{\mathcal{H}}\{\sigma_i',\sigma_i''\}=\sum_{\langle ij\rangle}\left[-\frac{J}{4}(\sigma_i'\sigma_j'+\sigma_i''\sigma_j'')-\frac{K}{4}\sigma_i'\sigma_i''\sigma_j'\sigma_j''+\frac{J}{4}(\sigma_i'\sigma_j''+\sigma_i''\sigma_j')+\frac{L}{2}(\sigma_i'\sigma_i''\sigma_j'-\sigma_i'\sigma_i''\sigma_j'')\right]$$

$$+\sum_i\left[\frac{(H+L)}{2}(\sigma_i'-\sigma_i'')-\frac{[D-T\ln(2)]}{2}\sigma_i'\sigma_i''\right]. \tag{30}$$

Note that we have dropped an unimportant constant in Eq. (30). The ln(2) factor in Eq. (30) appears because both the $(\sigma_i'=1,\sigma_i''=1)$ and $(\sigma_i'=-1,\sigma_i''=-1)$ states get mapped onto the same $S_i=0$ state.

A comparison of Eq. (30) with Eq. (1) shows that the two models are in general *not* the same. However, for the special case of $L=K=0$, the multispin interactions in Eq. (30) disappear. Furthermore, $\tilde{\Delta}=0$ is required in Eq. (1), which corresponds to $\Delta=0$ in the continuum limit (3). The parameters in Eq. (1) can then identified to be

$$J_1=-J/4,\quad J_2=-[D-T\ln(2)]/2,\quad J_3=J/4,\quad \tilde{\eta}=H/2. \tag{31}$$

If these conditions are met, the two models are not only equivalent for planar, but also—in the continuum limit—for *flexible* membranes, because the coupling to the mean curvature is taken to be the same in both cases.

The condition $L=K=0$ in Eq. (20) amounts to $b=a/4$ in the continuum Eq. (23) [23]. With these results, we find the relation between the parameters of the bilayer model and the three-component monolayer models to be

$$a'=-\lambda-\frac{a}{4}+T\ln(2), \tag{32}$$

$$b'=+\lambda-\frac{a}{4}-T\ln(2), \tag{33}$$

$$b_1'=b_1, \tag{34}$$

$$b_2'=0. \tag{35}$$

This shows in particular that the interaction potential between the lipids in the bilayer model corresponds to the chemical potential in the three-component model.

Phase diagrams of the three-component model with $b=a/4$ are shown in Fig. 6 for three different temperatures. Note that the phase diagrams have the same topology as that of the bilayer model given in Fig. 3. However, a direct comparison between the two models is only possible along a $\lambda=$const.-line in Fig. 6 and the $\Delta=0$-line in Fig. 3, with a' and b' determined by λ, compare Eqs. (32) and (33).

We compare the phase diagrams of the *same* system, calculated from the two models in the mean-field approximation for fixed values of the (corresponding) parameters a and λ. This is shown in Fig. 7. The two phase diagrams are very similar, as expected, but they are not identical. For example, there is a small downward shift of the critical temperature in the three-component monolayer. We believe that this difference is due to the fact that some degrees of freedom have been integrated out exactly in the three-component monolayer model, so that the mean-field approach implies different approximations in both cases.

V. DISCUSSION AND CONCLUSION

We have constructed simple models for two-component bilayer and three-component monolayer membranes. In the case of three-component monolayers, we assume that two components have spontaneous curvatures, which are equal in magnitude but of opposite sign, while the spontaneous cur-

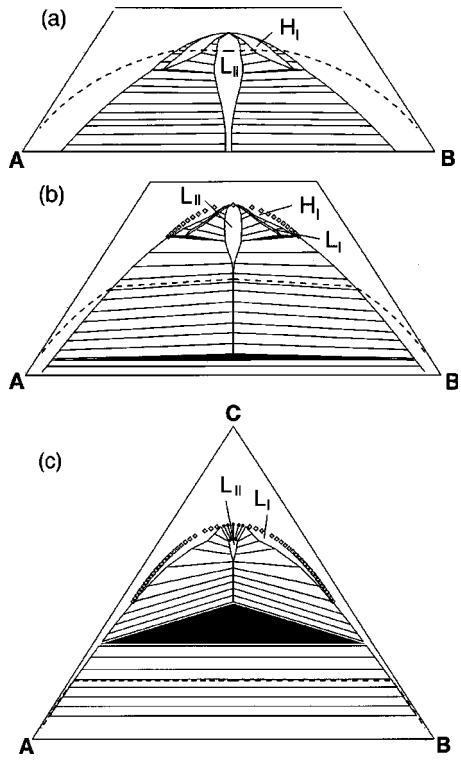

FIG. 6. Phase diagram of the three-component monolayer for $a=5.4$, $b=a/4$, $a_1=0.12$ and three different temperatures (a) $T=2$, (b) $T=1.5$, (c) $T=1.0$. Black areas indicate three-phase regions. The cut along the dashed line for $\lambda=2.7$ is shown in Fig. 7. The lines marked by diamonds ($\diamond$) indicate second-order transitions.

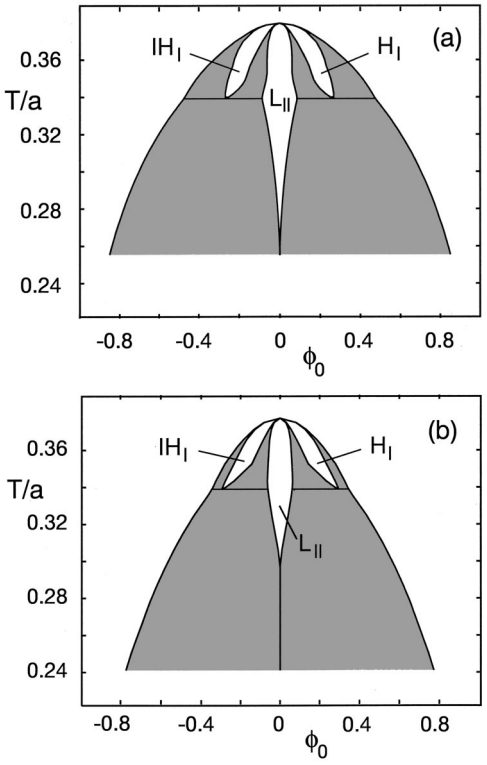

FIG. 7. Phase diagram in the $T-\phi$ plane of (a) two component bilayer with $\Delta=0$ and (b) three-component monolayer with $\lambda=2.7$ for $a=5.4$, $b=a/4$, $a_1=0.12$. See the text for the mapping of the parameters of the two models. Gray areas indicate two-phase regions.

vature of the third component vanishes. The resulting phase diagram of this model, calculated in the mean-field approximation, shows a rich phase behavior with three different modulated phases. In particular, we find that two different stripe phases can coexist. On the other hand, square phases are found to be only metastable in the weak segregation limit considered here.

The bilayer is modeled by coupling two monolayers with two different types of lipids. The resulting mean-field phase diagram is similar to that of three-component monolayer. A direct mapping between the two models exists in a special region of the parameter space.

The main result of our paper is that the total local concentration of the components in the two leaves of a bilayer is a thermodynamic variable, which cannot be integrated out to give a simpler model, which contains the concentration difference between the two layers only. Instead, the total concentration strongly affects the phase behavior. For equal concentration of A and B molecules in the two layers, the component with the larger overall concentration assembles in flat regions at the boundary between positively and negatively curved parts of the bilayer. If the concentrations in the two layers are sufficiently different, the domain structure is more pronounced in the monolayer, in which the concentration of the minority component is larger. Finally, when the total A- or B-concentration exceeds a threshold value, modulated phases no longer exist, and are replaced by a homogeneous, disordered phase.

Fluid-fluid phase separation has been studied intensively in amphiphilic monolayers at the water-air interface [24]. Such monolayers are almost *planar* since the interface exhibits a substantial tension, and can therefore not be used directly to study the phase behavior predicted in this paper. However, they indicate how phase separation should proceed in *flexible* monolayers containing several components. An interesting possibility is to study proteins, which are embedded in a two-component lipid monolayer. In one-component monolayers, adsorbed proteins have been found to accumulate at the boundary line between liquid-expanded and liquid-condensed domains [25].

In many cases, two-phase coexistence in *bilayers* is observed between a fluid and a gel phase [1,8]. In addition, some mixtures such as dielaidoyl PC/dipalmitoyl PE [26], phospholipid/cholesterol [27–30], and palmitoyl oleyl phosphatidyl serine (POPS)/didodecanoyl PC [31] exhibit two-phase coexistence regions where both phases are fluid. Fluid-fluid coexistence in two-component membranes is not necessarily restricted to mixtures of two lipids. Another possible scenario is proteins adsorbed to one side of a bilayer. If the proteins have an attractive interaction, there can be a phase separation into a protein-rich and a protein-pure phase.

The results of our model indicate two possible mechanisms for the formation of large domains in bilayers. First, a large concentration of one component in either one or both leaves of the bilayer leads to a homogeneous, disordered phase—even when the same system with equal concentrations of A and B undergoes phase separation. Second, at sufficiently large lateral tension, a variety of modulated phases becomes stable in a region of concentration space, where

macroscopic phase separation would occur if all components had zero spontaneous curvature. For small tensions, on the other hand, the membrane should undergo domain-induced budding which again acts to prevent the formation of large domains within the bilayer.

Compared to fluid-fluid coexistence, the two-phase coexistence between gel and fluid phases is more difficult to describe theoretically, since in general the shear elasticity of the gel domains has to be taken into account in addition to the curvature energy. However, the results calculated with the curvature energy alone still apply to the striped phases where the membranes are curved only in one direction and the shear energy vanishes. Furthermore, there are two additional features which make our results applicable to the gel-fluid coexistence region. First, because the coupling between shear stress and curvature is *quadratic* in the amplitude of the out-of-plane undulations, the shear energy should be small even for the hexagonal phases. Second, the gel phase often contains defects, and even a small density of dislocations makes the gel domains effectively fluidlike. Thus, we can speculate that our results provide an explanation for the percolation behavior observed in diffusion experiments at gel-fluid coexistence [32,33].

ACKNOWLEDGMENT

We thank T. Schilling for checking some of our numerical results independently.

[1] *Structure and Dynamics of Membranes—From Cells to Vesicles*, Vol. 1 of *Handbook of Biological Physics*, edited by R. Lipowsky and E. Sackmann (Elsevier, Amsterdam, 1995).
[2] G. Gompper and D. M. Kroll, Curr. Opin. Colloid Interface Sci. **2**, 373 (1997).
[3] R. Lipowsky, Curr. Opin. Struct. Biol. **5**, 531 (1995).
[4] L. Miao *et al.*, Phys. Rev. A **43**, 6843 (1991).
[5] U. Seifert, K. Berndl, and R. Lipowsky, Phys. Rev. A **44**, 1182 (1991).
[6] L. Miao, U. Seifert, M. Wortis, and H.-G. Döbereiner, Phys. Rev. E **49**, 5389 (1994).
[7] U. Seifert, Adv. Math. **46**, 13 (1997).
[8] M. D. Houslay and K. K. Stanley, *Dynamics of Biological Membranes* (Wiley, Chichester, 1990).
[9] H. Ringsdorf, B. Schlarb, and J. Venzmer, Angew. Chem. Int. Ed. Engl. **27**, 113 (1988).
[10] S. Leibler and D. Andelman, J. Phys. (France) **48**, 2013 (1987).
[11] R. Lipowsky, J. Phys. II **2**, 1825 (1992).
[12] F. Jülicher and R. Lipowsky, Phys. Rev. E **53**, 2670 (1996).
[13] T. Kawakatsu, D. Andelman, K. Kawasaki, and T. Taniguchi, J. Phys. II **3**, 971 (1993).
[14] H. Kodama and S. Komura, J. Phys. II **3**, 1305 (1993).
[15] T. Taniguchi, K. Kawasaki, D. Andelman, and T. Kawakatsu, J. Phys. II **4**, 1333 (1994).
[16] J. L. Harden and F. C. MacKintosh, Europhys. Lett. **28**, 495 (1994).
[17] F. C. MacKintosh and S. A. Safran, Phys. Rev. E **47**, 1180 (1993).
[18] F. C. MacKintosh, Phys. Rev. E **50**, 2891 (1994).
[19] P. L. Hansen, L. Miao, and J. H. Ipsen, Phys. Rev. E **58**, 2311 (1998).
[20] S. A. Safran, P. Pincus, and D. Andelman, Science **248**, 354 (1990).
[21] M. W. Matsen and F. S. Bates, Macromolecules **29**, 1091 (1996).
[22] M. Blume, V. Emery, and R. B. Griffiths, Phys. Rev. A **4**, 1071 (1971).
[23] D. Furman, S. Dattagupta, and R. B. Griffiths, Phys. Rev. B **15**, 441 (1977).
[24] S. Subramaniam and H. M. McConnell, J. Phys. Chem. **91**, 1715 (1987).
[25] R. R. Netz, D. Andelman, and H. Orland, J. Phys. II **6**, 1023 (1996).
[26] S. H. Wu and H. M. McConnell, Biochemistry **14**, 847 (1975).
[27] M. R. Vist and J. H. Davis, Biochemistry **29**, 451 (1990).
[28] P. F. F. Almeida, W. L. C. Vaz, and T. E. Thompson, Biochemistry **31**, 6739 (1992).
[29] J. L. Thewalt and M. Bloom, Biophys. J. **63**, 1176 (1992).
[30] M. Bloom and O. Mouritsen, in *Structure and Dynamics of Membranes—From Cells to Vesicles*, Vol. 1A of *Handbook of Biological Physics* (Ref. [1]), pp. 65–95.
[31] A. K. Hinderliter, J. Huang, and G. W. Feigenson, Biophys. J. **67**, 1906 (1994).
[32] P. F. F. Almeida and W. L. C. Vaz, in *Structure and Dynamics of Membranes—From Cells to Vesicles*, Vol. 1A of *Handbook of Biological Physics* (Ref. [1]), pp. 305–357.
[33] T. E. Thompson (private communication).